Chemical Engineering Journal 421 (2021) 129434

Contents lists available at ScienceDirect

Chemical Engineering Journal

journal homepage: www.elsevier.com/locate/cej

In situ kinetic studies of CVD graphene growth by reflection spectroscopy

C. Tsakonas [a], A.C. Manikas [a], M. Andersen [b], M. Dimitropoulos [a], K. Reuter [b,c], C. Galiotis [a,d,*]

[a] University of Patras, Chemical Engineering Department, 26504 Patras, Greece
[b] Chair for Theoretical Chemistry and Catalysis Research Center, Technische Universität München, Lichtenbergstr 4, 85747 Garching, Germany
[c] Fritz-Haber-Institut der Max-Planck-Gesellschaft, Faradayweg 4-6, 14195 Berlin, Germany
[d] Institute of Chemical Engineering Sciences, Foundation for Research and Technology Hellas (FORTH/ICE-HT), 26504 Patras, Greece

ARTICLE INFO

Keywords:
Graphene growth
Growth kinetics
Chemical vapour deposition
Reflectometry
Raman spectroscopy
Microkinetic modelling

ABSTRACT

Controllable large-scale synthesis of two-dimensional materials (2DMs) such as graphene is a prerequisite for industrial applications. Chemical vapor deposition (CVD) is currently the most widespread synthesis method as it is efficient and easy to automatize. The process itself is quite complex and poorly understood, but it is generally believed to involve a number of distinct steps such as hydrocarbon decomposition into surface-bound intermediates, diffusion on the catalytic substrate, generation of nucleation points and, finally, graphene growth. In situ monitoring and tailoring of such a complex procedure is beneficial for understanding the growth kinetics and, eventually, for controlling the graphene growth. Herein, we report on a novel metrology system based on *in situ* reflectance spectroscopy that has been developed for real-time monitoring of surface changes during graphene growth on Cu foils at high operating temperatures. The implementation of this technique for extracting kinetic parameters of the growth process is presented. Furthermore, a microkinetic model of graphene growth based on density-functional theory (DFT) and the hindered translator / rotator model for enthalpy and entropy corrections is constructed and used to obtain a microscopic understanding of the apparent activation energy and related rate-determining steps in graphene growth.

1. Introduction

Graphene is a perfect 2D crystal of covalently bonded carbon atoms and comprises the basis of all graphitic structures. Since its isolation in 2004 [1], it has attracted a great deal of scientific and technological interest because of its remarkable physical and mechanical properties, which result from its defect-free crystalline structure and the sp^2 hybridization. Monolayer graphene was first produced by micromechanical exfoliation [1] of highly oriented pyrolytic graphite (HOPG), but such a technique is time consuming, difficult to reproduce and provides only small amounts of high-quality graphene. Thus, large quantities of graphene sheets, required for most applications, cannot be obtained from this method.

Automated production of reasonable-quality graphene can be attained by CVD [2], which is currently the only available method that yields graphene of wafer dimensions. Furthermore, continuous growth by roll-to-roll methods has also been demonstrated recently [3,4]. The prospect of large-scale synthesis of graphene and other 2DMs via CVD has, indeed, facilitated the use of 2DMs in applications such as flexible electronics, gas sensors, energy storage etc. [5–7]. However, unlike mechanical exfoliation, the CVD graphene growth is a complex chemical process that involves a series of mass transport and surface reaction steps [8]. These are a) transport of gas-phase species (typically methane (CH_4) and hydrogen (H_2)) to and from the catalyst surface, b) methane adsorption and decomposition into hydrogen (which recombines on the surface to form H_2(g)) and active carbon or hydrocarbon species, c) diffusion of active species on the catalyst surface, d) generation of critical size nucleation points and, finally, e) epitaxial growth and merging of graphene domains to form a continuous graphene sheet.

The majority of graphene CVD processes employ as the catalyst polycrystalline Cu foils. To date, many theoretical [9–16] and experimental studies [17–21] have been conducted in order to elucidate the mechanism of graphene growth on Cu. In particular, aspects such as the role of hydrogen in CVD growth [9,11,15,16,20] , the rate-limiting steps [21], the role of carbon segregation versus surface adsorption [17], the concentrations of the reactants [22,23], and the overall pressure in the reactor (typically categorized as low-pressure (LP) or ambient-pressure (AP) CVD) [12] have been intensively discussed. Studies of the reaction mechanism often proceed by proposing a mechanism, which is then fit to available experimental data [14,21]. A major drawback of this

* Corresponding author.
E-mail address: c.galiotis@iceht.forth.gr (C. Galiotis).

https://doi.org/10.1016/j.cej.2021.129434
Received 27 November 2020; Received in revised form 12 March 2021; Accepted 16 March 2021
Available online 5 April 2021
1385-8947/© 2021 The Authors. Published by Elsevier B.V. This is an open access article under the CC BY license (http://creativecommons.org/licenses/by/4.0/).

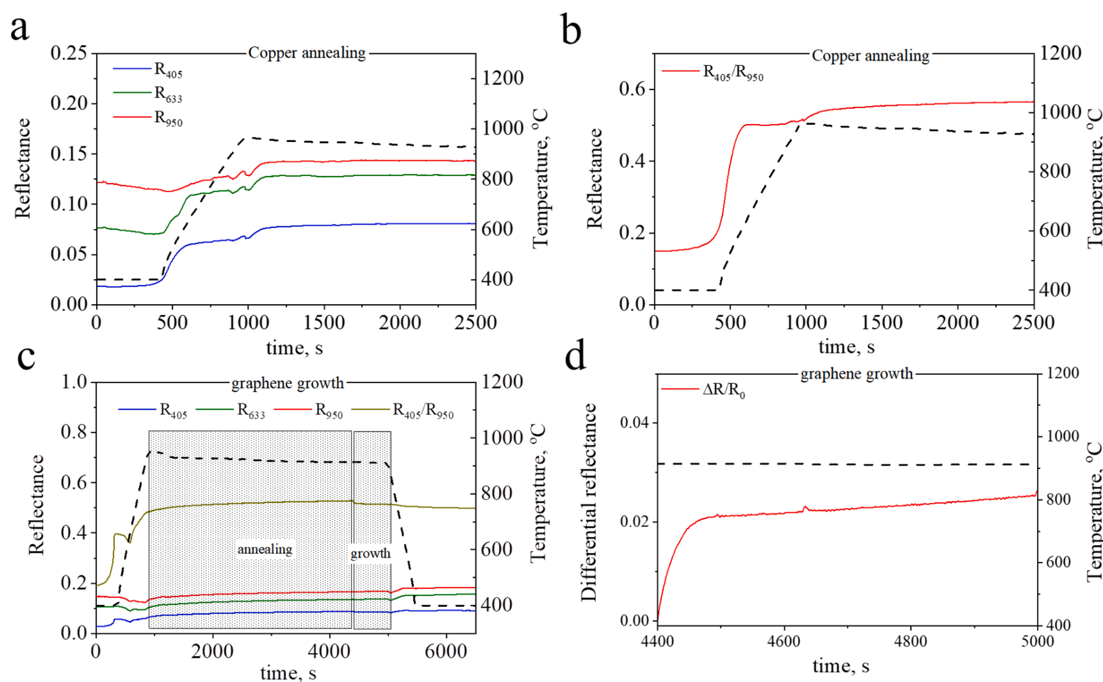

Fig. 1. In situ reflectance spectra recorded in the AIXTRON BM reactor as a function of time and temperature of (a) the 3 laser lines (405 nm, 633 nm and 950 nm) and (b) the R_{405}/R_{950} ratio during annealing of Cu foil, (c) the 3 laser lines (405 nm, 633 nm and 950 nm) and the R_{405}/R_{950} ratio for the combined annealing and graphene growth phases and (d) the differential reflectance during graphene growth. During the growth phase the partial pressures of methane and hydrogen were 0.04 and 2.27 mbar, respectively. The dashed black lines indicate the temperature (right y-axis).

approach is that fitting can provide a good description of the experiment even when based on wrong assumptions about e.g. the reaction mechanism or the active site model [24,25]. In general, it is often very difficult or even impossible to accurately measure the forward and reverse rate constants of individual reaction steps, especially for quite complex chemical reactions such as CVD graphene growth. This makes theoretical investigations, e.g. DFT calculations, invaluable as a supplement to experiments since they can provide independent estimates of thermodynamic and kinetic parameters such as the free energy of formation of possible surface intermediates as a function of the reaction conditions (temperature, gas-phase pressures) [16,26,27] or barriers for individual reaction steps [9,15].

Due to the complexity of the CVD process, it is vital to monitor and eventually control the stepwise reactions in order to tailor the final product to specific requirements. As mentioned above, the effects of various parameters such as temperature, pressure, precursor flow rate etc. upon CVD synthesis are not fully understood and most users rely on empirical recipes that are normally assessed by post-production (*ex situ*) characterization [28,29]. Most of the characterization techniques available at elevated temperatures are not easily adapted to *in situ* measurements though [30]. This is due to the spatial confinements of the reactor cell and the extreme experimental conditions. For instance, Raman spectroscopy, which is the main characterization tool operating in the visible, is challenging since black body radiation at high temperatures swarms the weak inelastic scattering. Certain limited reports for *in situ* characterization do exist, but they are primarily concerned with growth on nickel foils [31,32]. Losurdo *et al.* have e.g. used *in situ* spectroscopic ellipsometry (SE) to study the kinetics of graphene growth on nickel [31]. However, SE demands high structural stability, which is difficult to adjust to a CVD system. Lately, a number of studies on CVD growth of transition metal dichalcogenides employing *in situ* reflectance measurements have come to the front [33]. Other, albeit *ex situ*, differential reflectivity measurements have also been reported such as the work of Kaplas *et al.* on determining the thickness of graphene grown on Cu using room-temperature CVD [34].

In the work presented here we have embarked on a systematic campaign to assess the feasibility of *in situ* reflectometry at high operating temperatures in an attempt to retrieve useful information about the graphene quality and the reaction kinetics in real time. We have applied this technique to a conventional CVD furnace (see experimental) that co-feeds methane and hydrogen in Ar carrier gas on Cu foils at high temperatures (~1270K). Upon reaction initiation, reflectance fluctuations on the surface of Cu are monitored and analysed *in situ*. As demonstrated below, the collected data has helped us to understand the kinetics of the process and to quantify the number of graphene layers formed, and thus confirmed that differential reflectance spectroscopy can be employed for monitoring the growth in real time. Finally, by combining the experimental results with DFT-based computer simulations, we were able to show that the initial steps of methane decomposition are the rate-limiting steps and responsible for the apparent activation energy of the growth process of about 2.3–2.5 eV. The combined results also allow us to propose a new hypothesis about the role of hydrogen during CVD growth, namely that it acts as a catalyst activator at low hydrogen contents and as an etching agent at high hydrogen contents.

2. Materials and methods

CVD Growth. Graphene growth was performed in a commercially available cold wall CVD reactor (AIXTRON Black Magic Pro, Germany). For a typical process, polycrystalline Cu foil (JX Nippon Mining & Metals, 35 μm-thick, 99.95%) was cleaned by isopropanol to remove any organic contamination and then introduced into the CVD chamber. After the closure of the chamber and its pumping to 0.1 mbar, the Cu foil was annealed for 30 min in an environment of 10% of hydrogen in argon at a total pressure of 25 mbar at 1050 °C. The volumetric gas flow rates were adjusted with digital flowmeters for the highest possible accuracy. Afterwards, CH_4 was introduced into the chamber and the growth phase was initiated. The growth temperature was set between 1020 °C and 1070 °C.

Reflectometry. In situ reflection spectra were acquired with an EpiTT reflectometer supplied by Laytec and adapted to the AIXTRON

Table 1
Calculated reflectance for 405 nm and 950 nm of Cu and native Cu oxide/Cu substrates.

	405 nm	950
Cu	0.477	0.989
Native Cu oxide/Cu	0.213	0.984

CVD reactor. It is equipped with three different wavelengths (405 nm, 633 nm and 950 nm) generated by a high brightness LED light source which is delivered on the specimen surface through optical fibre. The spot size is 2.7 mm.

Raman spectroscopy. Raman microscopy was employed to assess ex situ the quality of the graphene grown on the CVD reactor. Raman spectra were collected with an InVia Renishaw spectrometer with 2400 & 1200 grooves/mm grating using a 100X lens (0.85NA) and a 514 nm excitation laser line. Laser power was 0.5 mW and acquisition time 10 s. Raman mapping has been performed on an area of 40x40 μm^2 at a step of 1 μm. All Raman peaks were fitted using Lorentzian functions.

3. Results and discussion

As discussed above, *in situ* reflectometry might be a useful tool to monitor the graphene growth process by retrieving information about the graphene quality and the reaction kinetics in real time. Fig. 1a shows a typical reflectance spectrum in which the changes of reflectance during annealing of the Cu foil are demonstrated. In brief, the main factors for the observed changes in reflectance are attributed to the reduction of the Cu surface and the morphological changes due to surface rearrangement. It is well known that an oxidized Cu foil reflects less compared to bare Cu [34,35], so the removal of surface Cu oxides during heating in 10% of hydrogen in Ar gas mixture should result in an increment of the reflectance intensity. Furthermore, at high temperatures the Cu surface becomes smooth because of the high mobility of the surface Cu atoms, which also results in higher reflectance values. When both processes are completed, the reflectance values reach a plateau since no more chemical or morphological changes beyond the steady-state thermal dynamics are occurring. Therefore, *in situ* reflectivity can be adopted for the control of the Cu substrate and for defining the appropriate starting point of the growth process. Regarding the different wavelengths employed in our experiments, based on theoretical calculations the 950 nm wavelength is almost unaffected by the reduction of the surface Cu oxides and thus the changes to the reflectance are probably due to the morphological changes on the surface. In contrast, the 405 nm reflectance is sensitive both to the changes in morphology, but also to the occurring chemical changes [34]. More detailed, the

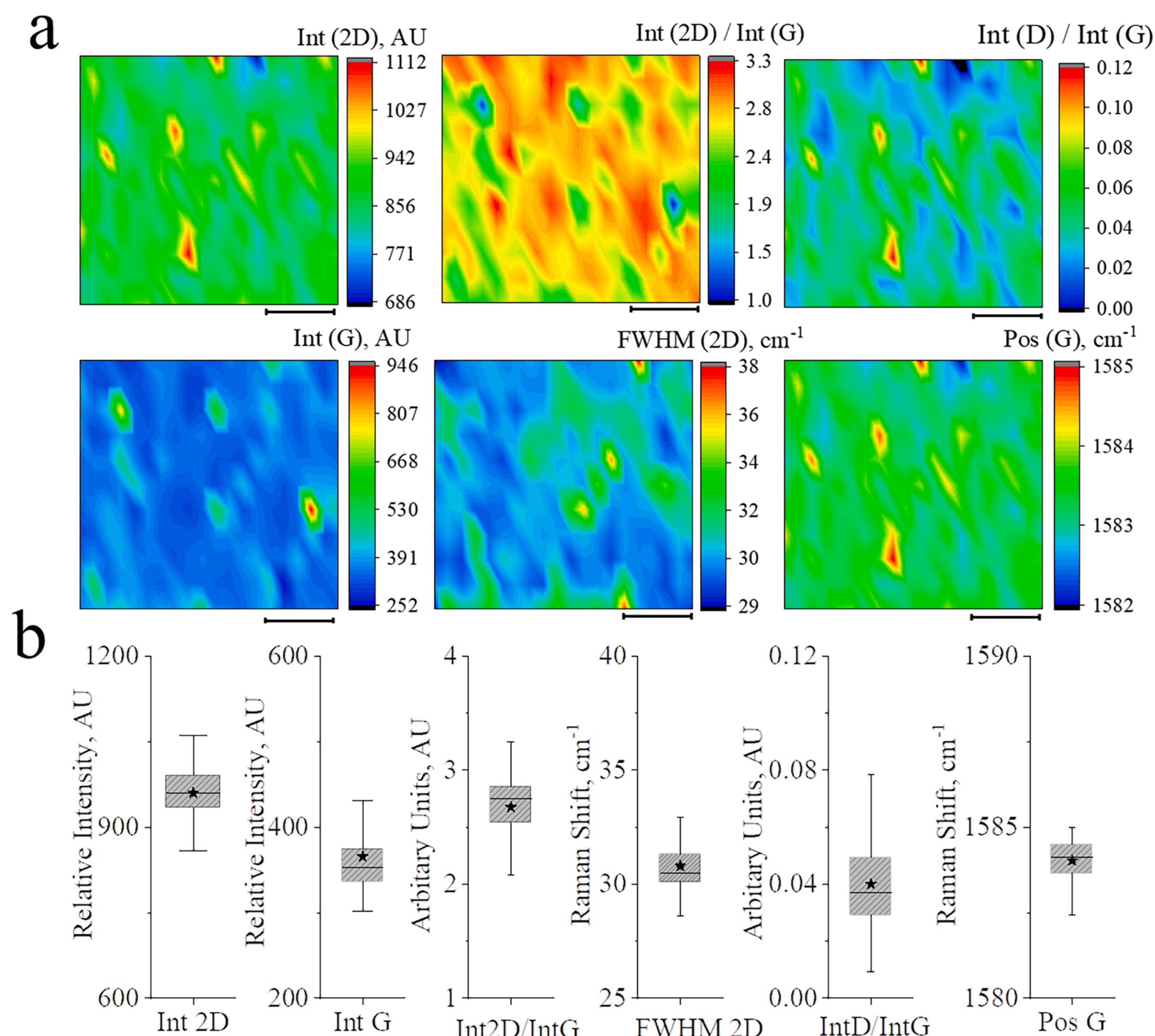

Fig. 2. (a) Ex situ Raman contours of Int(2D), Int(G), Int(2D)/Int(G), Int(D)/Int(G), FWHM(2D) and Pos(G) obtained from a CVD graphene sheet and (b) their statistical analysis. The scale bar is 10 μm.

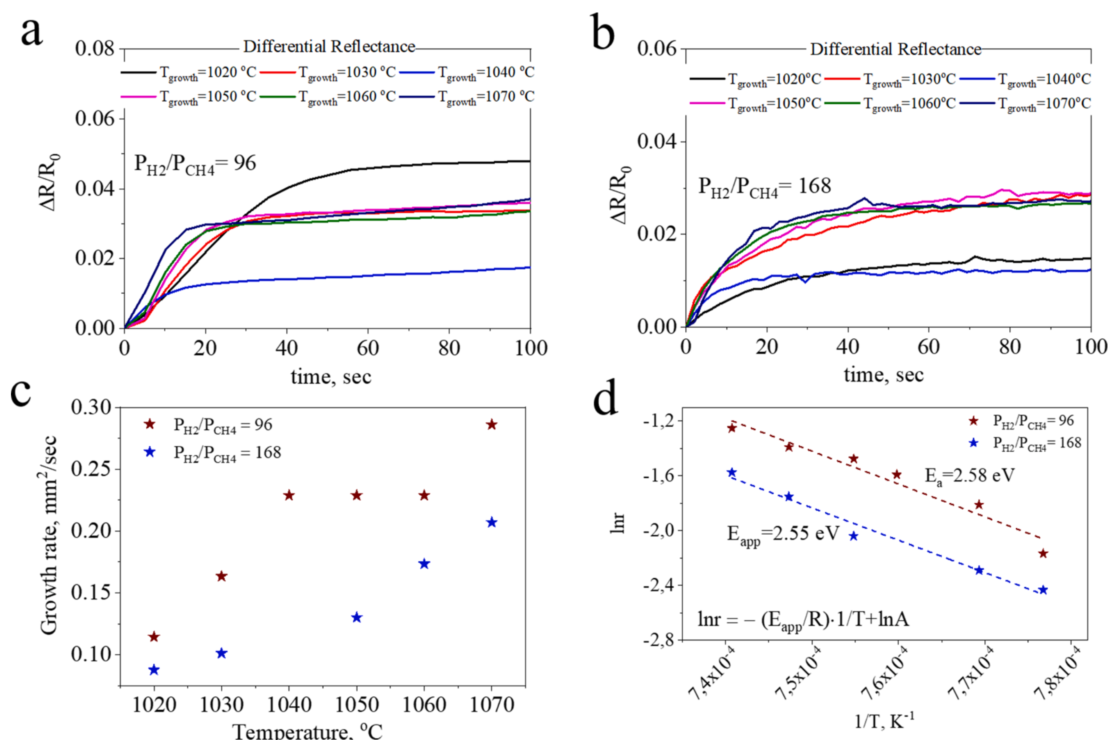

Fig. 3. The evolution of the differential reflectance $\Delta R/R_0$ with time during graphene growth for various growth temperatures and (a) $P_{H2}/P_{CH4} = 96$, (b) $P_{H2}/P_{CH4} = 168$. (c) The calculated average growth rates for the two different gas mixtures and (d) the natural logarithm of the growth rate, *r*, as a function of the inverse temperature (Arrhenius plot) with the derived apparent activation energy (E_{app}) for both cases.

reflectivity of a metal substrate coated with a homogeneous film of thickness h can be expressed by the following equation [34]:

$$R = \left| \frac{r_{12} + r_{23}\exp^{(2i\beta)}}{1 + r_{12}r_{23}\exp^{(2i\beta)}} \right|^2 \tag{1}$$

Here $r_{12} = \frac{(1-n_{\text{copper native oxide}})}{(1+n_{\text{copper native oxide}})}$, $r_{23} = \frac{(n_{\text{copper native oxide}}-n_{\text{copper}})}{(n_{\text{copper native oxide}}+n_{\text{copper}})}$, $\beta = \frac{2\pi n_{\text{copper native oxide}} {}^{*}h}{\lambda}$, h is the thickness of native copper oxide and λ is the laser wavelength.

By inserting the values of optical constants (refractive index n and extinction coefficient k) of copper [36] and native copper oxide (that is mainly Cu_2O and CuO) [37] (figure SX) to eq.1 and assuming that the thickness of native copper oxide is around 5 nm [38], the reflectance can be calculated. In table 1 the calculated values of reflectance for Cu and native Cu oxide at 405 nm and 950 nm are presented, respectively, in which it is clear that the reflectance at 950 nm wavelength is almost unaffected by the reduction of the surface Cu native oxides. In the case of 405 nm the changes to the reflectance are much more apparent and thus, this wavelength can be used to monitor the oxidation changes on the surface of Cu foil.

If we now assume that the effect of morphology upon the 405 nm and 950 nm reflectance is quite similar, we can use the ratio R_{405}/R_{950} as an index for the chemical changes occurring at the surface. The R_{405}/R_{950} ratio as a function of time and temperature is shown in Fig. 1b. The shape of the curve corroborates our initial assumption since the main transition occurs at around 400 °C, which is the critical temperature for the initiation of the reduction of the surface Cu oxides [35].

In Fig. 1c the evolution of the reflectance for all wavelengths (405 nm, 633 nm, 950 nm) and the R_{405}/R_{950} ratio are presented during both the annealing and graphene growth phases. As mentioned above, the R_{405}/R_{950} was employed so as to exclude the variation of the reflectance caused by morphological changes. In our case, when methane is fed to the reactor a slight decrease of the R_{405}/R_{950} ratio is observed due to the presence of graphene on the Cu surface. We ascribe this reduction of the reflectance to the different optical constants of graphene and Cu. In order to monitor the subtle changes occurring to the R_{405}/R_{950} ratio during graphene growth, we introduce the differential reflectance defined as the relative changes of the R_{405}/R_{950} ratio prior and after graphene growth.

$$\frac{\Delta R}{R_0} = \left| \frac{\frac{R_{Gr(405)}}{R_{Gr(950)}} - \frac{R_{Cu(405)}}{R_{Cu(950)}}}{\frac{R_{Cu(405)}}{R_{Cu(950)}}} \right|$$

The differential reflectance recorded during graphene growth, see Fig. 1d, shows a gradual increase with time followed by the formation of a plateau. Since, as discussed above, only chemical changes are recorded by the R_{405}/R_{950} ratio, the variation of the differential reflectance is clearly due to the emergence and growth of graphene on the surface. It is important to underline at this point that the most significant changes to the differential reflectance occur during the first seconds of the process, in agreement with previous work [39]. Comparing the experimental plateau values of the differential reflectance with those that have been derived from theoretical studies, aspects such as the quality of the graphene and the number of graphene layers can be investigated. In our case the grown graphene sheets seem to be monolayers as the found plateau value of around 2% is in good agreement with theoretical predictions for monolayer graphene (1.8%) (see SI). These results are of paramount importance and give us the opportunity for *in situ* monitoring of the quality and structural characteristics of graphene grown by CVD processes.

3.1. Quality control with Raman spectroscopy

With the objective to fully validate these present findings, we conducted *ex situ* Raman spectroscopy measurements on the grown graphene. The Raman spectrum of graphene consists of three main peaks; the G peak (~1582 cm^{-1}) which is present in all sp^2 carbon materials

and corresponds to the in-plane doubly degenerate Eg phonon in the center of Brillouin zone, the D peak which is activated by the presence of defects by a double resonant process of transverse optical phonons around the K-point of the Brillouin zone, and the 2D peak (second order of D peak) arising from a double resonant 2-phonon process, which does not require the presence of defects [40]. The combination of the D, G, and 2D peak characteristics, provides different information about graphene such as: (1) the defect density through the ratio of intensities of the D and G peaks (Int(D)/Int(G)) [41], (2) the number of layers through the full-width-half-maxima (FWHM) and shape of the 2D peak and the Int(2D)/Int(G) ratio and, finally, (3) the residual stresses through the positions of the G and 2D peaks (Pos(G), Pos(2D)) and the FWHM of the 2D peak [42,43]. Fig. 2 presents our detailed Raman mapping together with related statistical analysis of produced graphene that has previously been transferred onto a SiO_2 substrate. This investigation reveals that the sheet is continuous without cracks or tears in the examined area. The Int(D)/Int(G) ratio is found to be extremely small (~0.04), which confirms the low defect density of the produced graphene [41]. The presence of monolayer graphene throughout is confirmed through the Int(2D)/Int(G) ratio that takes the value of ~ 2.7 and the shape of the 2D peak, which is a single Lorentzian with FWHM around 31 cm^{-1} [40]. Finally, the presence of residual stresses in the grown graphene due to cooling from high temperatures and transfer can be determined by the shift of the G peak and was found to be compressive by −0.07% biaxial strain.

3.2. Growth kinetics

The recorded reflectance spectra can furthermore be used to extract information about the kinetics of graphene growth. This is of great interest since information in the literature is scarce and there is an evident industrial interest in kinetic control as it relates to automated production and energy consumption. As mentioned above, when the hydrocarbon source is fed to the reactor, the differential reflectance increases with time and after a while it reaches a plateau. This means that no more changes to the surface are occurring, and thus, it can be safely assumed that the growth has terminated. In Fig. 3a and b the values of $\Delta R/R_0$ as a function of time are presented for different experimental conditions characterized by the growth temperature and the ratio of the hydrogen and methane pressures (P_{H2}/P_{CH4}) fed to the reactor. It can be observed that the time it takes to reach the plateau depends on the experimental conditions, and this information has been used to calculate the average growth rate of graphene (Fig. 3c) for the different growth scenarios. As expected, it can be observed that the richer the methane gas mixture ($P_{H2}/P_{CH4} = 96$ vs 168) or the higher the temperature, the higher the growth rate. Fig. 3d shows the Arrhenius plots constructed based on the growth rates in Fig. 3c. From the slope of these plots we calculate values of the apparent activation energy E_{app} of 2.58 eV and 2.55 eV for the two gas ratios, respectively. These values are in good agreement with the value obtained by Kim *et al.* (2.6 ± 0.5 eV) in a previous experimental study that employed much more cumbersome *ex situ* scanning electron microscopy (SEM) characterization to obtain the growth rates (quantified through the area of the surface covered by graphene flakes after a defined growth time) [21,29]. Minor changes in the differential reflectance that are presented in Fig. 3 are due to minor fluctuations in graphene quality. It is widely known that CVD is a rather complex process [8,44] and even under exactly the same growth protocols, minor variations in graphene quality can be observed. For that reason, representative specimens have been tested ex-situ with Raman spectroscopy and, as expected, differences in peak G and 2D positions (Figs. S2, S3 and S4) and defect density (I_D/I_G) (Table ST2) can be observed. Those differences in graphene strain level and defect density affect the optical properties [45–48] and thus the reflectance characteristics.

3.3. Microkinetic modelling

In order to gain a microscopic understanding of the apparent activation energy and related rate-determining steps in graphene growth, we constructed a microkinetic model based on literature input parameters (energies and frequencies of important intermediates and transition states (TSs), see Supporting Information (SI) for details) calculated from DFT [9,15]. Previous detailed kinetic Monte Carlo (KMC) modelling of the entire graphene growth process on Cu(1 1 1) (including methane dissociation, surface diffusion, graphene nucleation and edge attachment) has shown that methane decomposition is likely the rate-determining step [15]. We therefore made use of a simplified effective reaction scheme that resolves only the methane decomposition steps and directly converts the decomposed product (a surface C atom) into graphene:

1) $CH_4(g) \rightleftharpoons CH_3{}^* + H^*$

2) $CH_3{}^* \rightleftharpoons CH_2{}^* + H^*$

3) $CH_2{}^* \rightleftharpoons CH^* + H^*$

4) $CH^* \rightleftharpoons C^* + H^*$

5) $C^* \rightleftharpoons C(g)$

6) $2H^* \rightleftharpoons H_2(g)$

Graphene is here modelled as a gas-phase species C(g) with highly negative free energy, i.e. it acts as a carbon sink that removes decomposed methane from the surface. This approximation allows us to solve the rate equations related to methane decomposition at steady state and to neglect all details related to how the graphene grows from the decomposed products. As a steady state solver, we here used the CatMAP software package [49].

The enthalpy and entropy corrections to the DFT energies are derived using the ideal gas approximation for the gas-phase species (methane and hydrogen) and the hindered translator / rotator (HTR) model proposed by Campbell *et al.* [50] for the adsorbates and TSs. The latter model is used as implemented in the ASE software package [51] with some minor additional implementations described in our previous work [16] and includes a more realistic representation of the potential energy landscape that takes into account diffusion and rotation barriers (further details are given in the SI). The refined corrections from the HTR model are highly important for modelling CVD growth of graphene on Cu, as temperatures are very high and many intermediates have very low diffusion and rotation barriers [16].

Following the standard approach, the enthalpies U and Gibbs free energies G are expressed as formation energies ΔU_f and ΔG_f with respect to methane and hydrogen according to the following equation (shown here for ΔG_f):

$$\Delta G_f(T, P_{H2}, P_{CH4}) = G_{Cu+ads}(T) - G_{Cu}(T) - G_{CH4}(T, P_{CH4}) - \left(\frac{y}{2} - 2\right) G_{H2}(T, P_{H2})$$

Here, G_{Cu+ads} and G_{Cu} are the Gibbs free energies of the adsorbate on the Cu surface and of the clean Cu surface, respectively, G_{CH4} and G_{H2} are the Gibbs free energies of methane and hydrogen, respectively, and y is the number of hydrogen atoms in the adsorbate. As discussed in detail in our previous work and in the ASE documentation, U contains the DFT-calculated formation enthalpies, the zero-point energy (ZPE) corrections as well as temperature-dependent corrections from the finite population of translational, rotational and vibrational modes. G furthermore contains the entropies of translational, rotational and vibrational modes and, for the gas-phase species, also pressure corrections to the entropy. Enthalpy and entropy corrections to the Cu surface are not taken into account, as these are assumed to be equal with and without the adsorbate.

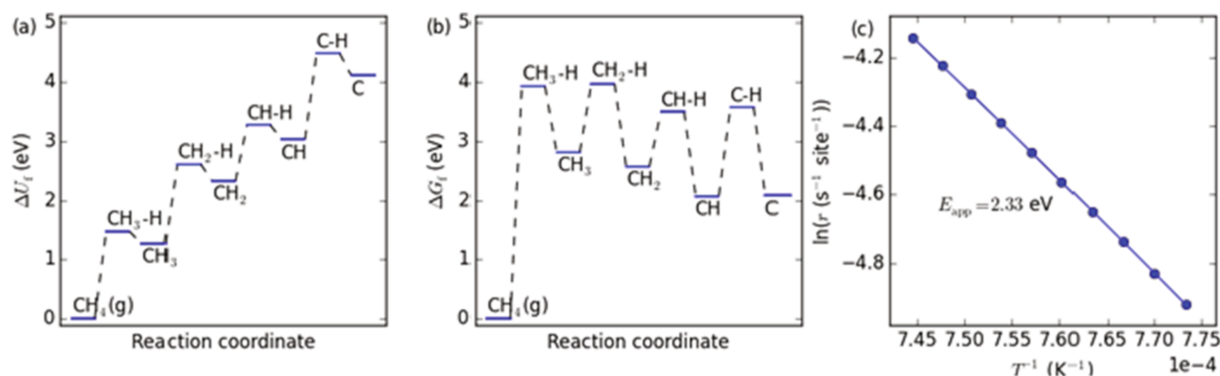

Fig. 4. Calculated formation enthalpies ΔU_f (a) and Gibbs free energies ΔG_f (b) of the intermediates and TSs involved in methane decomposition on Cu(1 1 1) using CH_4(g) and H_2(g) as reference. (c) Arrhenius plot calculated from the kinetic model in the experimentally covered temperature range (1293–1343 K) with derived theoretical apparent activation energy E_{app}. The temperature used in (a) and (b) is 1318 K and the gas-phase pressures used in (b) and (c) are 0.04 mbar for CH_4 and 6.7 mbar for H_2, which corresponds to the experimentally used pressures for the blue data points in Fig. 3d.

In Fig. 4a and b we show the calculated formation enthalpies and formation Gibbs free energies for the adsorbates and TSs involved in methane decomposition. Whereas the enthalpies show an increasing trend with the reaction progress, the free energies show a decreasing trend. The latter trend is caused by the highly negative free energy of the gas-phase hydrogen that is produced as the methane molecule decomposes. Note that hydrogen atoms adsorbed to Cu(1 1 1) are highly unstable and immediately recombine to form H_2(g) under CVD conditions, thus driving the reaction towards methane decomposition. The TSs for CH_4(g) and CH_3* decomposition have almost equal Gibbs free energies and represent the highest free energy barriers to be overcome along the reaction pathway. As confirmed by actually solving the microkinetic model and calculating Campbell's degree of rate control (DRC) X_i [52] (see below), these are indeed the rate-determining steps.

In Fig. 4c we show the Arrhenius plot calculated by solving the microkinetic model over the experimentally covered temperature range. From the slope the theoretical apparent activation energy E_{app} is calculated to be 2.33 eV, which is in quite good agreement with the experimental value of about 2.55 eV derived above. E_{app} can be related to the

$$\mathrm{DRCs}X_iX_i = \left(\frac{\partial(\ln r)}{\partial\left(-\Delta G_{f,i}/RT\right)}\right)_{\Delta G_{f,j\neq i}}$$

(where r is the reaction rate and R is the gas constant) and formation enthalpies $\Delta U_{f,i}$ of the adsorbates and TSs i using the following formula proposed by Campbell *et al.* [53]:$E_{app} = RT + \sum_i X_i \Delta U_{f,i}$

We find that the only species with non-negligible ($\mathrm{abs}(X_i) > 0.02$) DRC are the TSs for CH_4(g) and CH_3* decomposition, for which we find values of about 0.4 (CH_3-H) and 0.6 (CH_2-H). The corresponding $\Delta U_{f,i}$ values are 1.48 eV (CH_3-H) and 2.61 eV (CH_2-H). E_{app} is thus found to have a value that is in between the formation enthalpies of the CH_3-H and CH_2-H TSs (plus the small RT correction that amounts to 0.11 eV at 1318 K) since these are the TSs of the dominant rate-determining steps. It should be noted here that when several reaction steps are rate-determining, the apparent activation energy is highly sensitive to small changes to the energetics. A perfect agreement with the experimentally measured E_{app} of 2.55 eV could in fact be achieved by either increasing the enthalpy of the CH_2-H TS or decreasing the enthalpy of the CH_3-H TS by only 0.1 eV. Uncertainties of this order of magnitude are within the expected DFT error (typically estimated as around 0.2 eV [54]), and we can therefore conclude that the theoretical E_{app} is in very good agreement with experiment within the model uncertainties. Also, the exact partial pressures used can lead to small changes to E_{app}. For instance, when using the methane and hydrogen partial pressures corresponding to the red data points in Fig. 3d ($P_{H2}/P_{CH4} = 96$) we obtain an E_{app} of 2.56 eV, which is however still in very good agreement with experiment. We note that Kim *et al.* excluded methane decomposition as the rate-determining step and origin of their measured E_{app} based on the DFT-calculated activation enthalpies (barriers) of the methane decomposition steps, which are all significantly lower (around 1.7–1.9 eV) than the measured E_{app} [21,29]. However, as we have shown here this apparent discrepancy can be resolved by realizing that E_{app} in fact depends on the formation enthalpies (with respect to gas-phase methane and hydrogen) of the rate-determining methane decomposition TSs (as explained through the formula proposed by Campbell *et al.* [53]), and not on the barriers of the individual steps. The danger of simply equating experimentally measured E_{app} values with individual activation barriers of elementary steps has been highlighted before [53,55].

Apart from the apparent activation energy, it is also interesting to compare the actual growth rate predicted from the kinetic model with experiment. A rough estimate of the time it would take to form a complete graphene monolayer can be made from the inverse of the theoretical reaction rate (with units per site per second), thereby assuming that every decomposed methane molecule immediately covers its reaction site with graphene. For the considered temperature range this results in times of 60–130 s, which is in quite good agreement with the times required to reach the plateau in the experimental data in Fig. 3b. However, since the theoretical model does not take into account the slowdown of the growth rate as the graphene begins to cover the active surface sites, it may be more appropriate to compare it to the experimental values derived using only the initial, linear part of the experimental growth curves. This analysis is presented in the SI and would lead to an experimental apparent activation energy of 2.13 eV (Fig. S5) and growth times of around 30 s, which, however still remains within the uncertainties of the theoretical model, considering that a typical DFT error of 0.2 eV would lead to an uncertainty in the growth time of about a factor of five at 1318 K. In this connection, we note that we also carried out test calculations using the simpler harmonic approximation as implemented in ASE for the free energy corrections of the adsorbates and TSs (not shown), which, however did not lead to results that could be reconciled with experiment within the estimated model uncertainties. As stated above, appropriately accounting for diffusion and rotation barriers through the HTR model is thus imperative at the high growth temperatures. We further note that previous modelling results have suggested that graphene growth may proceed directly from the partially decomposed CH intermediate, instead of from the surface C atom [15]. Our results change very little if this alternative mechanism is considered, as the CH decomposition is not one of the dominant rate-determining steps. However, the fact that the C and CH intermediates are observed to have very similar Gibbs free energies (see Fig. 4b) corroborates that CH could indeed be an important active species for the further graphene growth.

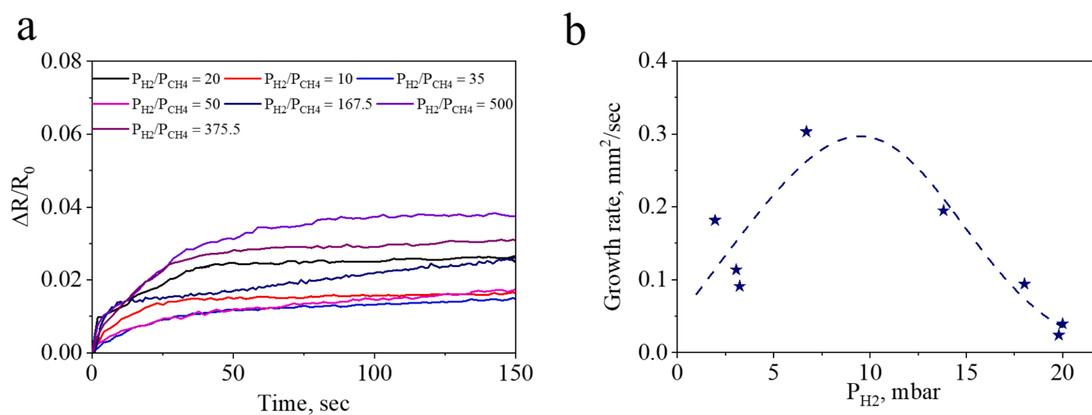

Fig. 5. (a) The evolution of the differential reflectance $\Delta R/R_0$ with time during graphene growth for different hydrogen partial pressure and (b) the calculated growth rate. The methane partial pressure was kept constant at 0.04 mbar and the growth temperature was 1050 °C.

3.4. Role of hydrogen

Another important open question in graphene CVD growth concerns the role of hydrogen, which is typically co-fed into the reactor together with the hydrocarbon reactant during graphene growth. Vlassiouk *et al.* employed *ex situ* SEM characterization to investigate the effect of the hydrogen partial pressure on the reaction rate and found a 'bell-shaped' dependence where intermediate hydrogen pressures gave rise to a maximum in the growth rate [56]. Our unique *in situ* monitoring capabilities and the resulting quantification of the differential reflectance during the growth allow us study the influence of the hydrogen pressure on the growth kinetics at much reduced experimental effort (see Fig. 5a) and to confirm the 'bell-shape' of the curve (see Fig. 5b). Vlassiouk *et al.* speculated that active hydrogen atoms on the Cu surface might promote the activation of physisorbed methane and thereby cause the initial increase of the reaction rate with the hydrogen pressure at low hydrogen content. However, in view of our detailed investigation of the chemical and morphological changes that occur at the Cu surface during the initial catalyst preparation phase where Cu is annealed in a hydrogen-rich atmosphere, we find it more likely that the primary role of hydrogen at very low hydrogen contents is to keep the catalyst surface in its activated state. Oxygen (but also other contaminants) that might be present in the gasses fed to the reactor passivate the Cu surface active sites and thereby reduce its catalytic activity. Therefore, we speculate that the presence of hydrogen removes surface contamination such as oxides and thereby improves the catalytic activity of the Cu surface, resulting in increasing growth rates. On the other hand, when the hydrogen concentration is high it mainly acts as an etching reagent and thus causes a reduction in the growth rate. This second declining part of the curve in Fig. 5b can also be reproduced with our microkinetic model (see Fig. S6). We also note that the concentration of atomic hydrogen at the Cu(1 1 1) surface obtained in our microkinetic model is extremely low ($8 \cdot 10^{-3}$ per Cu site), which thus makes it unlikely that surface hydrogen atoms should influence the kinetics of methane adsorption as proposed by Vlassiouk *et al* [56].

4. Conclusions

In this study we demonstrated the viability of a novel metrology system based on *in situ* reflectance spectroscopy to retrieve information about the graphene quality and the reaction kinetics during the CVD growth process on Cu foils. We found that the completion of the growth process can be identified by the reflectance reaching a plateau, the value of which allowed us to determine that monolayer graphene had been produced. The latter was further confirmed by *ex situ* Raman spectroscopy that revealed the characteristics of a continuous monolayer sheet with a low number of defects. The *in situ* monitoring capabilities furthermore allow for the efficient investigation of the influence of a number of growth parameters such as the temperature and the methane and hydrogen partial pressures on the growth kinetics. A good agreement with previous results obtained from much more tedious and indirect *ex situ* investigations was found for the apparent activation energy and the dependence of the growth rate on the hydrogen partial pressure. We provided a new interpretation of the microscopic origin of these experimental observations through the establishment of a reductionist first-principles microkinetic model for graphene growth. In particular, we showed that the sole consideration of the methane dissociation steps is sufficient to obtain a good agreement with both the experimental apparent activation energy and the overall growth rate. This implies that the subsequent diffusion and growth steps are likely not rate-determining, which was also the conclusion reached in a recent detailed KMC study [15]. These latter steps could, nevertheless, still be important for other characteristics of graphene growth such as the shapes of the grown flakes [10]. The value of the apparent activation energy (about 2.3–2.5 eV) could be explained from the finding that the first two dissociation steps (i.e. the steps from CH_4(g) to surface-bound CH_2*) are both partly rate-limiting. Furthermore, the combined experimental and theoretical results led us to propose that hydrogen plays a rather complex role in the CVD process, i.e. it acts as a catalyst activator at low hydrogen contents and as an etching reagent at high hydrogen contents. Our results thus offer a detailed understanding of graphene growth via CVD and highlight that differential reflectance spectroscopy is a vital tool for *in situ* characterization and monitoring of the growth.

Declaration of Competing Interest

The authors declare that they have no known competing financial interests or personal relationships that could have appeared to influence the work reported in this paper.

Acknowledgements

This FET-Open project has received funding from the European Union's Horizon 2020 research and innovation program 'Development of continuous two-dimensional defect-free materials by liquid-metal catalytic Routes' under grant agreement 736299. Responsibility for the information and views set out in this article lies entirely with the authors. Aixtron Ltd. (Cambridge, UK), and Laytec AG, Germany are also acknowledged for technical support and useful advice. The publication of this article has been financed by the Research Committee of the University of Patras.

Appendix A. Supplementary data

Supplementary data to this article can be found online at https://doi.org/10.1016/j.cej.2021.129434.

References

[1] K.S. Novoselov, A.K. Geim, S.V. Morozov, D. Jiang, Y. Zhang, S.V. Dubonos, I. V. Grigorieva, A.A. Firsov, Electric field effect in atomically thin carbon films, Science 306 (2004) 666.

[2] X. Li, W. Cai, J. An, S. Kim, J. Nah, D. Yang, R. Piner, A. Velamakanni, I. Jung, E. Tutuc, S.K. Banerjee, L. Colombo, R.S. Ruoff, Large-area synthesis of high-quality and uniform graphene films on copper foils, Science 324 (2009) 1312.

[3] E.S. Polsen, D.Q. McNerny, B. Viswanath, S.W. Pattinson, A. John Hart, High-speed roll-to-roll manufacturing of graphene using a concentric tube CVD reactor, Sci. Rep. 5 (2015) 10257.

[4] G. Zhong, X. Wu, L. D'Arsie, K.B.K. Teo, N.L. Rupesinghe, A. Jouvray, J. Robertson, Growth of continuous graphene by open roll-to-roll chemical vapor deposition, Appl. Phys. Lett. 109 (2016), 193103.

[5] P. Miró, M. Audiffred, T. Heine, An atlas of two-dimensional materials, Chem. Soc. Rev. 43 (18) (2014) 6537–6554.

[6] S.Z. Butler, S.M. Hollen, L. Cao, Y.i. Cui, J.A. Gupta, H.R. Gutiérrez, T.F. Heinz, S. S. Hong, J. Huang, A.F. Ismach, E. Johnston-Halperin, M. Kuno, V.V. Plashnitsa, R. D. Robinson, R.S. Ruoff, S. Salahuddin, J. Shan, L.i. Shi, M.G. Spencer, M. Terrones, W. Windl, J.E. Goldberger, Progress, challenges, and opportunities in two-dimensional materials beyond graphene, ACS Nano 7 (4) (2013) 2898–2926.

[7] X. Li, Y. Zhu, W. Cai, M. Borysiak, B. Han, D. Chen, R.D. Piner, L. Colombo, R. S. Ruoff, Transfer of large-area graphene films for high-performance transparent conductive electrodes, Nano Lett. 9 (12) (2009) 4359–4363.

[8] R. Muñoz, C. Gómez-Aleixandre, Review of CVD synthesis of graphene, Chem. Vap. Deposition 19 (10-11-12) (2013) 297–322.

[9] P. Li, Z. Li, J. Yang, Dominant kinetic pathways of graphene growth in chemical vapor deposition: The role of hydrogen, J. Phys. Chem. C 121 (46) (2017) 25949–25955.

[10] E. Meca, V.B. Shenoy, J. Lowengrub, H 2 -dependent attachment kinetics and shape evolution in chemical vapor deposition graphene growth, 2D Materials 4 (2017) 031010.

[11] W. Zhang, P. Wu, Z. Li, J. Yang, First-Principles Thermodynamics of graphene growth on Cu surfaces, J. Phys. Chem. C 115 (36) (2011) 17782–17787.

[12] S. Bhaviripudi, X. Jia, M.S. Dresselhaus, J. Kong, Role of kinetic factors in chemical vapor deposition synthesis of uniform large area graphene using copper catalyst, Nano Lett. 10 (10) (2010) 4128–4133.

[13] G. Gajewski, C.-W. Pao, Ab initio calculations of the reaction pathways for methane decomposition over the Cu (111) surface, J. Chem. Phys. 135 (2011), 064707.

[14] H. Kim, E. Saiz, M. Chhowalla, C. Mattevi, Modeling of the self-limited growth in catalytic chemical vapor deposition of graphene, New J. Phys. 15 (2013), 053012.

[15] J. Li, G. Liu, B. Ren, E. Croiset, Y. Zhang, L. Ricardez-Sandoval, Mechanistic study of site blocking catalytic deactivation through accelerated kinetic Monte Carlo, J. Catal. 378 (2019) 176–183.

[16] M. Andersen, J.S. Cingolani, K. Reuter, Ab initio thermodynamics of hydrocarbons relevant to graphene growth at solid and liquid Cu surfaces, J. Phys. Chem. C 123 (36) (2019) 22299–22310.

[17] X. Li, W. Cai, L. Colombo, R.S. Ruoff, Evolution of graphene growth on Ni and Cu by carbon isotope labeling, Nano Lett. 9 (12) (2009) 4268–4272.

[18] Y. Zhang, Z. Li, P. Kim, L. Zhang, C. Zhou, Anisotropic hydrogen etching of chemical vapor deposited graphene, ACS Nano 6 (1) (2012) 126–132.

[19] B. Hu, Y. Jin, D. Guan, Z. Luo, B. Shang, Q. Fang, H. Ruan, H2-dependent carbon dissolution and diffusion-out in graphene chemical vapor deposition growth, J. Phys. Chem. C 119 (42) (2015) 24124–24131.

[20] M. Losurdo, M.M. Giangregorio, P. Capezzuto, G. Bruno, Graphene CVD growth on copper and nickel: role of hydrogen in kinetics and structure, PCCP 13 (46) (2011) 20836, https://doi.org/10.1039/c1cp22347j.

[21] H. Kim, C. Mattevi, M.R. Calvo, J.C. Oberg, L. Artiglia, S. Agnoli, C.F. Hirjibehedin, M. Chhowalla, E. Saiz, Activation energy paths for graphene nucleation and growth on Cu, ACS Nano 6 (4) (2012) 3614–3623.

[22] Z. Luo, Y. Lu, D.W. Singer, M.E. Berck, L.A. Somers, B.R. Goldsmith, A.T. C. Johnson, Effect of substrate roughness and feedstock concentration on growth of wafer-scale graphene at atmospheric pressure, Chem. Mater. 23 (6) (2011) 1441–1447.

[23] J. Kraus, L. Böbel, G. Zwaschka, S. Günther, Understanding the reaction kinetics to optimize graphene growth on cu by chemical vapor deposition, Ann. Phys. 529 (2017) 1700029.

[24] M.K. Sabbe, M.-F. Reyniers, K. Reuter, First-principles kinetic modeling in heterogeneous catalysis: An industrial perspective on best-practice, gaps and needs, Catal. Sci. Technol. 2 (2012) 2010–2024.

[25] K. Reuter, C.P. Plaisance, H. Oberhofer, M. Andersen, Perspective: On the active site model in computational catalyst screening, J. Chem. Phys. 146 (2017), 040901.

[26] S. Chen, J. Gao, B.M. Srinivasan, G. Zhang, V. Sorkin, R. Hariharaputran, Y.-W. Zhang, An all-atom kinetic Monte Carlo model for chemical vapor deposition growth of graphene on Cu(1 1 1) substrate, J. Phys.: Condens. Matter 32 (15) (2020) 155401.

[27] S. Chen, J. Gao, B.M. Srinivasan, G. Zhang, V. Sorkin, R. Hariharaputran, Y.-W. Zhang, A kinetic Monte Carlo model for the growth and etching of graphene during chemical vapor deposition, Carbon 146 (2019) 399–405.

[28] H.C. Lee, W.-W. Liu, S.-P. Chai, A.R. Mohamed, A. Aziz, C.-S. Khe, N.M.S. Hidayah, U. Hashim, Review of the synthesis, transfer, characterization and growth mechanisms of single and multilayer graphene, RSC Advances 7 (2017) 15644-15693.

[29] L. Lin, B. Deng, J. Sun, H. Peng, Z. Liu, Bridging the gap between reality and ideal in chemical vapor deposition growth of graphene, Chem. Rev. 118 (18) (2018) 9281–9343.

[30] C. Tsakonas, M. Dimitropoulos, A.C. Manikas, C. Galiotis, Growth and in situ characterization of 2D materials by chemical vapour deposition on liquid metal catalysts: A review, Nanoscale 13 (6) (2021) 3346–3373.

[31] M. Losurdo, M.M. Giangregorio, P. Capezzuto, G. Bruno, Ellipsometry as a real-time optical tool for monitoring and understanding graphene growth on metals, J. Phys. Chem. C 115 (44) (2011) 21804–21812.

[32] F.S. Al-Hazmi, G.W. Beall, A.A. Al-Ghamdi, A. Alshahrie, F.S. Shokr, W. E. Mahmoud, Raman and ellipsometry spectroscopic analysis of graphene films grown directly on Si substrate via CVD technique for estimating the graphene atomic planes number, J. Mol. Struct. 1118 (2016) 275–278.

[33] Y. Wang, L. Zhang, C. Su, H. Xiao, S. Lv, F. Zhang, Q. Sui, L. Jia, M. Jiang, Direct Observation of Monolayer MoS(2) Prepared by CVD Using In-Situ Differential Reflectance Spectroscopy, Nanomaterials (Basel, Switzerland) 9(11) (2019) 1640.

[34] T. Kaplas, A. Zolotukhin, Y. Svirko, Thickness determination of graphene on metal substrate by reflection spectroscopy, Opt. Express 19 (18) (2011) 17226.

[35] J.Y. Kim, J.A. Rodriguez, J.C. Hanson, A.I. Frenkel, P.L. Lee, Reduction of CuO and Cu2O with H2: H embedding and kinetic effects in the formation of suboxides, J. Am. Chem. Soc. 125 (2003) 10684–10692.

[36] P.B. Johnson, R.W. Christy, Optical constants of the noble metals, Phys. Rev. B 6 (12) (1972) 4370–4379.

[37] J.J. Díaz León, D. Fryauf, R. Cormia, N. Kobayashi, Study of the formation of native oxide on copper at room temperature, SPIE2016 9924 (2016).

[38] I. Platzman, R. Brener, H. Haick, R. Tannenbaum, Oxidation of polycrystalline copper thin films at ambient conditions, J. Phys. Chem. C 112 (4) (2008) 1101–1108.

[39] R. Forker, M. Gruenewald, T. Fritz, Optical differential reflectance spectroscopy on thin molecular films, Ann. Rep. Sec. C Phys. Chem. 108 (2012) 34–68.

[40] L.M. Malard, M.A. Pimenta, G. Dresselhaus, M.S. Dresselhaus, Raman spectroscopy in graphene, Phys. Rep. 473 (5-6) (2009) 51–87.

[41] A. Eckmann, A. Felten, A. Mishchenko, L. Britnell, R. Krupke, K.S. Novoselov, C. Casiraghi, Probing the nature of defects in graphene by Raman spectroscopy, Nano Lett. 12 (8) (2012) 3925–3930.

[42] A.C. Manikas, M.G. Pastore Carbone, C.R. Woods, Y. Wang, I. Souli, G. Anagnostopoulos, M. Hadjinicolaou, K.S. Novoselov, C. Galiotis, Stress transfer at the nanoscale on graphene ribbons of regular geometry, Nanoscale 11 (30) (2019) 14354–14361.

[43] M.G. Pastore Carbone, A.C. Manikas, I. Souli, C. Pavlou, C. Galiotis, Mosaic pattern formation in exfoliated graphene by mechanical deformation, Nat. Commun. 10 (2019) 1572.

[44] C. Mattevi, H. Kim, M. Chhowalla, A review of chemical vapour deposition of graphene on copper, J. Mater. Chem. 21 (10) (2011) 3324–3334.

[45] Z. Peng, X. Chen, Y. Fan, D.J. Srolovitz, D. Lei, Strain engineering of 2D semiconductors and graphene: from strain fields to band-structure tuning and photonic applications, Light Sci. Appl. 9 (2020) 190.

[46] G.G. Naumis, S. Barraza-Lopez, M. Oliva-Leyva, H. Terrones, Electronic and optical properties of strained graphene and other strained 2D materials: a review, Rep. Prog. Phys. 80 (9) (2017) 096501.

[47] M. Shakourian-Fard, G. Kamath, The effect of defect types on the electronic and optical properties of graphene nanoflakes physisorbed by ionic liquids, PCCP 19 (6) (2017) 4383–4395.

[48] J.-H. Zhong, J. Zhang, X. Jin, J.-Y. Liu, Q. Li, M.-H. Li, W. Cai, D.-Y. Wu, D. Zhan, B. Ren, Quantitative correlation between defect density and heterogeneous electron transfer rate of single layer graphene, J. Am. Chem. Soc. 136 (47) (2014) 16609–16617.

[49] A.J. Medford, C. Shi, M.J. Hoffmann, A.C. Lausche, S.R. Fitzgibbon, T. Bligaard, J. K. Nørskov, CatMAP: A software package for descriptor-based microkinetic mapping of catalytic trends, Catal. Lett. 145 (2015) 794–807.

[50] L.H. Sprowl, C.T. Campbell, Líney Árnadóttir, Hindered translator and hindered rotor models for adsorbates: Partition functions and entropies, J. Phys. Chem. C 120 (18) (2016) 9719–9731.

[51] A. Hjorth Larsen, J. Jørgen Mortensen, J. Blomqvist, I.E. Castelli, R. Christensen, M. Dułak, J. Friis, M.N. Groves, B. Hammer, C. Hargus, E.D. Hermes, P.C. Jennings, P. Bjerre Jensen, J. Kermode, J.R. Kitchin, E. Leonhard Kolsbjerg, J. Kubal, K. Kaasbjerg, S. Lysgaard, Jón Bergmann Maronsson, T. Maxson, T. Olsen, L. Pastewka, A. Peterson, C. Rostgaard, J. Schiøtz, O. Schütt, M. Strange, K. S. Thygesen, T. Vegge, L. Vilhelmsen, M. Walter, Z. Zeng, K.W. Jacobsen, The atomic simulation environment—A python library for working with atoms, J. Phys.: Condens. Matter. 29 (27) (2017) 273002.

[52] C. Stegelmann, A. Andreasen, C.T. Campbell, Degree of rate control: How much the energies of intermediates and transition states control rates, J. Am. Chem. Soc. 131 (2009) 8077–8082.

[53] Z. Mao, C.T. Campbell, Apparent activation energies in complex reaction mechanisms: A simple relationship via degrees of rate control, ACS Catal. 9 (2019) 9465–9473.

[54] A.J. Medford, J. Wellendorff, A. Vojvodic, F. Studt, F. Abild-Pedersen, K. W. Jacobsen, T. Bligaard, J.K. Nørskov, Assessing the reliability of calculated catalytic ammonia synthesis rates, Science 345 (2014) 197.

[55] H. Meskine, S. Matera, M. Scheffler, K. Reuter, H. Metiu, Examination of the concept of degree of rate control by first-principles kinetic Monte Carlo simulations, Surf. Sci. 603 (10-12) (2009) 1724–1730.

[56] I. Vlassiouk, M. Regmi, P. Fulvio, S. Dai, P. Datskos, G. Eres, S. Smirnov, Role of hydrogen in chemical vapor deposition growth of large single-crystal graphene, ACS Nano 5 (7) (2011) 6069–6076.